Journal of Solid Mechanics Vol. 8, No. 2 (2016) pp. 326-333

Application of the GTN Model in Ductile Fracture Prediction of 7075-T651 Aluminum Alloy

S.F. Hosseini , S. Hadidi-Moud *

Department of Mechanical Engineering, Ferdowsi University of Mashhad, Mashhad , Iran

Received 22 February 2016; accepted 12 April 2016

ABSTRACT

In this paper the capability of Gurson-Tvergaard-Needleman (GTN) model in the prediction of ductile damage in 7075-T651 aluminum alloy is investigated. For this purpose, three types of specimens were tested: Standard tensile bars, Round notched bar (RNB) specimens and compact tension (C(T)) specimens. Standard tensile bar tests were used to obtain the mechanical properties of the material and to calibrate the independent parameters of GTN model. RNB and C(T) specimen test results were used for validation of the calibrated parameters. Finite element analyses were carried out using ABAQUS commercial software for two purposes; calibration of the GTN model parameters and validation of the model predictions. The comparison between the finite element analyses and the test results suggested that the GTN model is capable of damage prediction in notched specimens, but not a good in cracked specimens. Finally, To show the applicability of the model in industry-level problems, the model is used for damage predictions of internal pressure vessels made of 7075-t651 aluminum alloy.

Keywords : Ductile fracture; GTN model; Calibrated parameters; 7075-T651 aluminum alloy.

1 INTRODUCTION

EXHIBITING excellent mechanical properties has placed 7075 aluminum alloys amongst the widely used engineering materials in light weight structures especially in the aircraft and aerospace industry. Careful examinations of fractured surfaces of components made of this material using scan electron microscopy have revealed that under quasi static loading conditions, although a rather abrupt fracture incident is often observed, the mechanism of fracture is mainly ductile and failure takes place through nucleation, growth and coalescence of micro-voids [1]. More specifically the ductility of the alloy is typically governed by the nucleation of the primary voids [2]. The secondary void nucleation and growth also occurs at smaller sized particles. Finally void coalescence takes place by the joining of primary and secondary voids. Although the major cause of damage is due to primary voids the nucleation and growth from secondary voids would reduce the ductility. Therefore, due to the leading role of these features in description of fracture, it is anticipated that a Gurson-Tvergaard-Needleman (GTN) model [3] should provide an appropriate explanation of the fracture event in great details.

Chang-Kyun Oh et al. [4] have used the GTN model to present a phenomenological model of ductile fracture for the API X65 steel. Their experimental tests and finite element damage simulations on notched bar tests and cracked bend bar tests showed that this model is capable of predicting ductile failure of defective pipes made of API X65. In

*Corresponding author. Tel.: +98 935 306 5949.
E-mail address: hadidi@um.ac.ir (S. Hadidi-Moud).

a study by S. Acharyya et al., [5], The GTN model and it is calibrated parameters were used to simulate the load versus load point displacement and crack growth for pipe with circumferential crack under four point bending made of 22NiMoCr37 steel. They concluded that GTN model is capable of predicting ductile fracture at the component level. S. Chiluvern [6] used GTN model to predict crack initiation in cross-roll piercing. N. Benseddiq et al. [7] collected some sets of GTN parameters calibrated for different materials. There are researchers who applied GTN model to modify cleavage fracture predictions in the transition temperature region of a ferritic steel where the number of cleavage initiation sites decreases due to preceding ductile void formation [8]. The GTN model was also used to describe damage progression in friction stir welded aluminum [9], small punch test [10] and hemming process [11]. Special attentions has been paid to Forming Limit Diagram (FLD) of aluminum alloys, for example H. Min et al. [12] predicted the forming limit stress diagram of Aluminum Alloy 5052 based on GTN model parameters determined by In Situ tensile test. Also the main objective of the work done by L. Xiao [13] was to experimentally and numerically evaluate the forming limit curve (FLC) of aluminum alloy 2B06. As another industry-level application, the GTN model was successfully applied in bursting prediction of hydroforming aluminum alloy tube [14].

Implementation of GTN model in the finite element program, ABAQUS, provided a numerical way to calibrate its parameters. In the next section, a brief description of GTN model is presented. This was followed by the outline of the experimental program. Results of experiments were then used in the finite element analyses to obtain the GTN model parameters for this material. Finally the RNB and C(T) test results were used for validation of the calibrated parameters for this material.

2 THE GTN MODEL

2.1 Structure

In 1977 Gurson [15] suggested a way to reach an appropriate yield surface for a voided material. The Garson's yield function described by the following equation:

$$\Phi = \left(\frac{\sigma_{eq}}{\sigma_y}\right)^2 + 2f\,.\cosh\left(\frac{3\sigma_m}{2\sigma_y}\right) - 1 - f^{\,2} = 0 \tag{1}$$

where σ_{eq} is the equivalent Von Mises stress, σ_m and σ_y refer to the mean stress the yield stress of the material respectively. Also f is the void volume fraction which is defined as the ratio of the total volume of all cavities to the volume of the body. Considering the interaction between adjacent holes, Tvergaard [16] introduced q_1 and q_2 parameters to modify the yield surface. Furthermore, Tvergaard and Needleman [3] substituted the void volume fraction f in the original equation by a modified void volume fraction f^* in order to account for the loss of load bearing capacity due to the void coalescence. Considering the above modifications, the Eq. (1) changes to:

$$\Phi = \left(\frac{\sigma_{eq}}{\sigma_y}\right)^2 + 2q_1 f^*.\cosh\left(\frac{3q_2\sigma_m}{2\sigma_y}\right) - 1 - (q_1 f^{*2}) = 0 \tag{2}$$

and the function f^* is given by:

$$f^*(f) = \begin{cases} f & f \le f_c \\ f_c + \dfrac{f_u^* - f_c}{f_f - f_c}(f - f_c) & f \succ f_c \end{cases} \tag{3}$$

where f_c and f_f are the critical void volume fraction and the void volume fraction at total failure respectively and f_u^* sets to $1/q_1$, so the modified void volume fraction f^* corresponds to the void volume fraction f unless the critical porosity f_c is exceeded.

It should be pointed out that for $q_1 = q_2 = 1$, the Eq. (2) reduces to Eq. (1) and if f is set to zero, the material would be without any porosity and the Garson's yield function reduces to the Von Mises yield function.

Since change in porosity of the material is due to the combination of growth and nucleation, the evolution of void volume fraction is given by:

$$\dot{f} = \dot{f}_{growth} + \dot{f}_{nucleation} \tag{4}$$

where $\dot{f}_{growth}$ is the change due to the growth of existing voids and $\dot{f}_{nucleation}$ is the change due to the nucleation of new voids. The law of conservation of mass requires:

$$\dot{f}_{growth} = (1-f)\dot{\varepsilon}_p : I \tag{5}$$

where $\dot{\varepsilon}_p$ is the plastic volume dilatation rate. Nucleation is assumed to be strain controlled and normally distributed in the following manner:

$$\dot{f}_{nucleation} = A\,\dot{\varepsilon}_e^{pl} \tag{6}$$

where $\dot{\varepsilon}_e^{pl}$ is the equivalent plastic strain and

$$A = \frac{f_N}{S_N\sqrt{2\pi}} \exp\left\{-\frac{1}{2}\left[\frac{\varepsilon_e^{pl} - \varepsilon_N}{S_N}\right]^2\right\} \tag{7}$$

Nucleation strain is normally distributed with mean value ε_N and standard deviation S_N as parameters. f_N is the maximum void volume fraction of nucleated voids.

The explained GTN model has 8 independent parameters (ε_N ,S_N ,f_N ,f_c ,f_f ,f_0 ,q_1 and q_2) which should be calibrated by means of comparing the experimental load-displacement curve obtained from standard test specimens with the simulated load-displacement results. The GTN model is implemented in ABAQUS commercial code and an explicit solver has to be used for simulations. A detailed explanation of this procedure is presented in the next section.

3 THE EXPERIMENTAL PROGRAM

3.1 Material

To obtain the yield properties of the material and calibrate the parameters of the GTN model, tensile tests were carried out for three standard tensile bars using ASTM B557 standard test method for aluminum bars [17]. The results obtained from the three specimens were almost identical. Fig. 1 shows the resulted true stress- true strain curve.

Using Fig. 1, the mechanical properties of the material were obtained as shown in Table 1.

The load-displacement data obtained from these standard tensile tests was then used to calibrate the GTN model parameters through comparison with the FE analysis results.

Table1
Mechanical properties of material.

E[Gpa]	S_y [Mpa]	S_{ut} [Mpa]	Fracture strain[%]
71	363	420	6.23

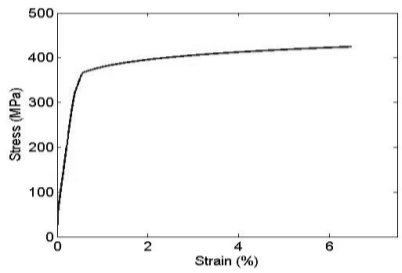

Fig.1
True stress - True strain curve.

3.2 RNB and C(T) Testing

Because of the need to validate our predictions, tests were carried out on RNB and C(T) specimens. Table 2. shows geometrical details of the RNB specimens.

As typical examples, details of two RNB specimens, 13-0.15 and 13-4.4 are shown in Fig. 2 and the load-displacement results for RNB9-1.1 specimens are plotted in Fig. 3.

Moreover, three identical CT specimens were tested using ASTM E399 standard with $w = 13mm$ and $\frac{a}{w} = 0.5$ [18]. Fig. 4 displays the load displacement curves obtained from CT testing. A Zwick testing machine was used for all experiments and specimens were loaded under displacement controlled loading at a constant rate of 1 mm/min. The parameter used to compare the experimental findings with the FE results was "displacement at failure". The values of this parameter for all RNB and C(T) specimens are listed in Table 3.

Table2
The specifications of RNB specimens.

Specimen name	D[mm]	d (net section) [mm]	Radius[mm]	Number of specimens
9-0.15	18	9	0.15	3
13-0.15	18	13	0.15	3
9-1.1	18	9	1.1	3
13-1.1	18	13	1.1	3
9-4.4	18	9	4.4	3
13-4.4	18	13	4.4	3

Table 3
The values of displacements at total failure.

Specimen name	Displacement at failure [mm]			Mean
	Specimen 1	Specimen 2	Specimen 3	
9-0.15	0.1907	0.2025	0.2159	0.2030
13-0.15	0.3517	0.3656	0.4127	0.3766
9-1.1	0.3746	0.3992	0.4144	0.3937
13-1.1	0.5534	0.4622	0.5184	0.5113
9-4.4	0.5580	0.4983	0.5334	0.5299
13-4.4	0.8447	1.0759	1.0915	1.0040
CT	2.2	2.35	2.8	2.45

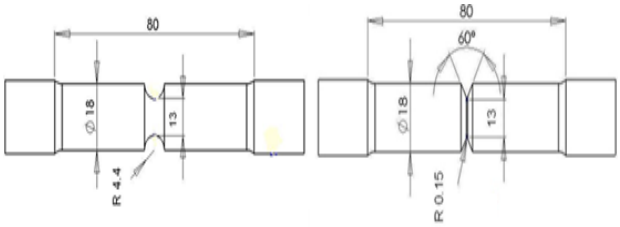

(a) (b)

Fig.2
A complete description of two RNB specimens: (a) 13-4.4 and (b) 13-0.15.

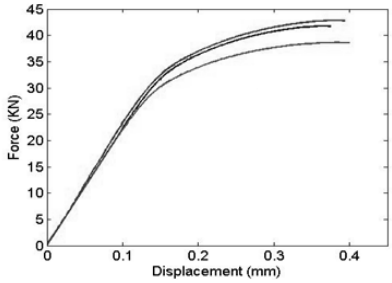

Fig.3
Load-displacement curves of RNB 9-1.1 specimens.

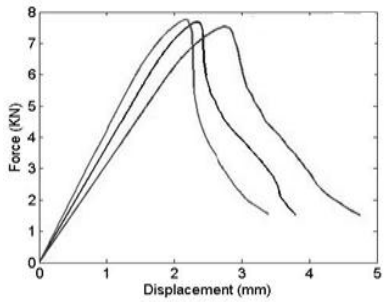

Fig.4
Load-displacement curves of C(T) specimens.

4 FE ANALYSES AND CALIBRATION

Elastic-Plastic finite element damage analyses based on GTN model were undertaken for the standard tensile bars. ABAQUS version 6.9 was used for all FE simulations. Axial symmetry conditions of RNB specimens allowed the use of axisymmetric meshes for standard tensile bars. The preliminary GTN parameters chosen from literature [7] were considered as initial estimates for the material model and were changed based on a step by step improvement procedure in order to get the best fit between the experimental load-displacement curve and simulated load-displacement curve. Table 4. reported some GTN model parameters based on ref [7]. The generated axisymmetric FE model of the standard tensile bar is shown in Figs. 5(a) and 5(b) displays the best fit between the simulated and experimental curves using the final calibrated GTN parameters listed in Table 5.

It should be noted that since the calibrated parameters are empirical no unique set of parameters can be claimed [4].

Table 4
The GTN model parameters of some materials [7].

Material	ε_N	S_N	f_N	f_c	f_f	f_0	q_1	q_2
C-Mn Steel	-	-	-	0.004	-	0.002	1.5	-
20MnMoNi5	0.3	0.1	0.04	0.02	1.141	0.001	1.5	-
22NiMoCr37	0.3	0.1	0.004	0.033	0.15	0.002	1.15	-
AL- Al_2 Ti	0.5	0.2	0.04	0.02	0.34	0	1.5	-
E690	0.3	0.1	0.00085	0.035	0.15	0.0015	1.5	-

Table 5
Calibrated parameters of GTN model.

Calibrated parameters	ε_N	S_N	f_N	f_c	f_f	f_0	q_1	q_2
	0.2	0.075	0.04	0.01	0.2	0.0085	1.5	1

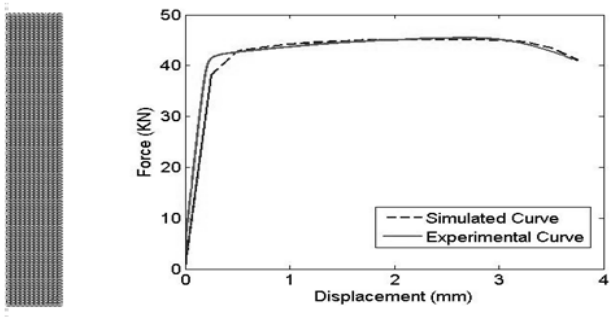

(a) (b)

Fig.5
(a) Axisymmetric model of standard tensile bar and (b) The best fit between FE and experimental load-displacement curves.

5 VALIDATION AND RESULTS

Now, for validation purposes we apply the set of calibrated parameters to RNB and CT models in order to find out the displacement loads at failure. The findings were compared with the test results shown in Table 6. The mesh size in validation specimens should be refined properly. This is important because the distance between the centers of two adjacent meshes is considered to be the distance between the two adjacent voids. It is crucial that the mesh size in RNB and CT models should be almost the same as that of standard tensile bar model which is already used in the calibration procedure. The condition of fracture for the RNB models is the loss of load carrying capacity of all elements at the net section area. This condition for CT model considered to be the loss of load carrying capacity of all elements at the crack front region. Figs. 6(a) and 6(b) show the failure conditions for 13-0.15 RNB model and CT model respectively. Table 6. shows the simulated failure displacements of RNB and CT specimens. The test results are listed again in this table for comparison.

Table 6
Comparison between simulation and experimental displacements at fracture.

Specimen name	Displacement at failure [mm]		Error (%)
	Experiment (mean)	Simulation	
9-0.15	0.2030	0.2300	13.3
13-0.15	0.3766	0.3826	1.6
9-1.1	0.3937	0.3890	1.2
13-1.1	0.5113	0.5398	5.6
9-4.4	0.5299	0.4535	14.4
13-4.4	1.0040	0.9405	5.95
CT	2.45	1.75	28.6

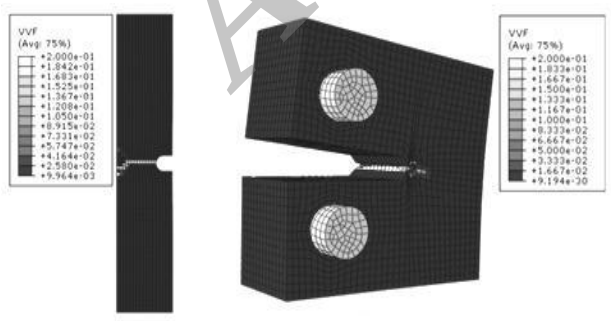

(a) (b)

Fig.6
Fracture conditions (a) 13-4.4 specimen and (b) CT specimen.

6 AN INDUSTRY- LEVEL APPLICATION

As an industrial example, the application of model in design and damage prediction of a thick cylindrical pressure vessel made of 7075-T651 aluminum alloy is presented. Light weight, excellent corrosion resistance, and the ability to transmit heat rapidly are only a few of the benefits of aluminum pressure vessels. Fig. 7 shows the meshed axisymmetric model of cylindrical pressure vessel with elastic-plastic-damage parameters equal to that of RNB and CT specimens. The outer diameter, thickness and length of this vessel are 0.1m, 1.2m and 1m respectively. One can easily predict the total failure of vessel considering the current void volume fraction and critical/total void volume fraction of material. For the above mentioned vessel, at a pressure of about 92 MPa, the total void volume fraction of 0.2 is reached. Fig. 8 shows the void volume fraction distribution in pressure vessel subjected to the internal pressure of 92 MPa.

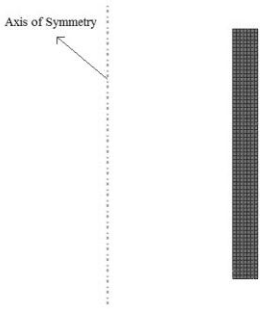

Fig.7
Meshed axisymmetric model of pressure vessel.

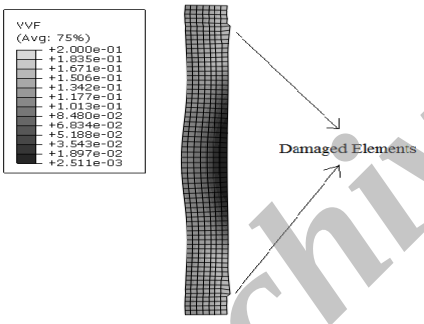

Fig.8
Void Volume Fraction Distribution in the pressure vessel thickness

7 CONCLUSIONS

The results shown in Table 6. suggest that for the case of RNB specimens, the ductile damage prediction of GTN model for 7075-T651 aluminum alloy is relatively good. In the other hand, damage predictions for CT specimens seem to be conservative. For CT specimens, the use of special fixtures for the tests would influence the load point displacements. It is therefore anticipated that the use of CMOD parameter instead of displacement, would lead to better results.

We also have to mention that based on Table 6., there is no trend which shows the dependency of the errors to the notch radius of specimens. This may mean that cleavage features play an important role in the fracture event of 7075-T651 aluminum alloy specimens and components. The GTN model cannot take this into consideration. The presence of both ductile and brittle mechanisms in a total fracture of 7075 aluminum alloy was proved from metallurgical point of view (see ref [19]), considering the fact that based on geometry and loading rates, one is more dominant.

Based on fairly good validation results especially for notched specimens, the model was applied to damage prediction in internal pressure vessels to show the applicability of model in industry-level problems. The designer may use critical or total void volume fraction to design the geometry parameters or to calculate the maximum allowable pressure.

REFERENCES

[1] Jordon J. B., 2009, Damage characterization and modeling of a 7075-T651 aluminum plate, *Materials Science and Engineering* **527**: 169-178.

[2] Fabregue D., Pardoen T., 2008, A constitutive model for elastoplastic solids and secondary voids, *Journal of the Mechanics and Physics of Solids* **56**: 719-741.

[3] Tvergaard V., Needlemann A., 1984, Analysis of the cup-cone fracture in a round tensile bar, *Acta Metallurgica* **32**: 57-69.

[4] Chang-Kyun O., 2007, A phenomenological model of ductile fracture for API X65 steel, *Internatinal Journal of Mechanical Science* **49**: 1399-1412.

[5] Acharyya S., Dhar S., 1999, A complete GTN model for prediction of ductile failure of pipe, *Journal of Materials Science* **43**: 1897-1909.

[6] Chiluverin S., 2007, *Computational Modeling of Crack Initiation in Cross-roll Piercing*, MSc Thesis, Massachusetts Institute of Technology.

[7] Benseddiq N., Imad A., 2008, A ductile fracture analysis using a local damage model, *International Journal of Pressure Vessels and Piping* **85**: 219-227.

[8] Bernauer G., Brocks W., Schmitt W., 1999, Modifications of the beremin model for cleavage fracture in the transition region of a ferritic steel, *Engineering Fracture Mechanics* **64**: 305-325.

[9] Nielsen K. L., 2008, Ductile damage development in friction stir welded aluminum (AA2024) joints, *Engineering Fracture Mechanics* **75**: 2795-2811.

[10] Abendorth M., Kuna M., 2006, Identification of ductile damage and fracture parameters from the small punch test using neural networks, *Engineering Fracture Mechanics* **73**: 710-725.

[11] Maout N. L., Thuillier S., Manach P. Y., 2009, Aluminum alloy damage evolution for different strain paths – application to hemming process, *Engineering Fracture Mechanics* **76**: 1202-1214.

[12] He M., Li F., Wang Z., 2011, Forming limit stress diagram prediction of aluminum alloy 5052 based on GTN model parameters determined by in situ tensile test, *Chinese Journal of Aeronautics* **24**: 378-386.

[13] Li X., Song N., Guo G., 2012, Experimental measurement and theoretical prediction of forming limit curve for aluminum alloy 2B06, *Transactions of Nonferrous Metals Society of China* **22**: 335-342.

[14] Teng B., Wang W., Liu Y., Yuan S., 2014, Bursting prediction of hydroforming aluminum alloy tube based on Gurson-Tvergaard-Needleman damage model, *Procedia Engineering* **81**: 2211- 2216.

[15] Gurson A. L., 1977, Continuum theory of ductile rupture by void nucleation and growth: part I – yield criteria and flow rules for porous ductile media, *Journal of Engineering Materials and Technology* **99**(1): 2-15.

[16] Tvergaard V., 1982, On localization in ductile materials containing spherical voids, International Journal of Fracture **18**: 37-52.

[17] *Annual Book of ASTM Standard*, 1997, Standard test methods for tension testing of wrought and cast aluminum- and magnesium-alloy products, ASTM B557-10.

[18] *Annual Book of ASTM Standard*, 1997, Standard test method for plane strain fracture toughness of metallic materials , ASTM E-399-90.

[19] Tajally M., Huda Z., Masjuki H. H., 2010, A comparative analysis of tensile and impact-toughness behavior of cold-worked and annealed 7075 aluminum alloy, *International Journal of Impact Engineering* **37**: 425-432.